

Multi-information fusion based localization algorithm for Mars rover

Xiuqiang Jiang^a, Shuang Li^{*}, Ting Tao^b and Bingheng Wang^c

College of Astronautics, Nanjing University of Aeronautics and Astronautics, Nanjing 210016, China

(Received April 13, 2014, Revised June 17, 2014, Accepted June 20, 2014)

Abstract. High-precision autonomous localization technique is essential for future Mars rovers. This paper addresses an innovative integrated localization algorithm using a multiple information fusion approach. Firstly, the output of IMU is employed to construct the two-dimensional (2-D) dynamics equation of Mars rover. Secondly, radio beacon measurement and terrain image matching are considered as external measurements and included into the navigation filter to correct the inertial basis and drift. Then, extended Kalman filtering (EKF) algorithm is designed to estimate the position state of Mars rovers and suppress the measurement noise. Finally, the localization algorithm proposed in this paper is validated by computer simulation with different parameter sets.

Keywords: Mars rover; localization; multi-information fusion; radio measurement; terrain image matching; extended Kalman filter

1. Introduction

With the capabilities of autonomous surface roaming and exploration, Mars rover is a high-precision autonomous robot, which can travel for several kilometers or even further on the complex and unstructured surface of Mars. Therefore, the surface environment and specific scientific objectives on Mars can be directly surveyed through the onboard scientific instruments of Mars rovers. Some basic functions are essential for Mars rover long-range roaming exploration, such as independent path planning, localization, obstacle avoidance, and motion control, etc. (Bajracharya *et al.* 2008). Key to the success of the Mars roaming exploration missions is the localization algorithm, which is required to determine the rover position information in a specified navigation reference coordinate system (Di *et al.* 2008). The position information is not only a prerequisite for path planning but also an important input for the sub-systems of obstacle avoidance and motion control. It also provides important support for creating the roaming terrain map, safe traveling and exploring the interested areas as much as possible within its lifetime. Furthermore, the capability of all-weather high-precision localization is required to accomplish the

*Corresponding author, Professor, E-mail: lishuang@nuaa.edu.cn

^aPh.D. Student, E-mail: jiangxq@nuaa.edu.cn

^bGraduate Student, E-mail: 940191815@qq.com

^cUndergraduate Student, E-mail: 694020988@qq.com

future exploration missions on the surface of Mars, especially on complex dangerous terrain but with high scientific value, which presents some new challenges (Wang 2008, Karahayit 2010, Gong 2013).

Currently, Mars rovers are usually operated by remote command and telemetry using the deep-space network (DSN), which has two aspects of deficiencies. The one is that, Mars rovers may be unobservable for DSN because of the rotation and revolution of Earth and Mars. At the same time, there is a larger communication delay between Mars and Earth (Bajracharya *et al.* 2008, Di *et al.* 2008). Therefore, NASA and European Space Agency (ESA) are fastening much attention on developing the innovative localization technologies for future Mars rover missions (Wang 2008, Karahayit 2010, Gong 2013).

Generally, Mars rover autonomous localization approaches mainly include inertial navigation (dead reckoning), celestial navigation, radio measurement, visual navigation, terrain image matching localization. Inertial navigation has the advantage of high autonomy, but the performance degrades with time due to the inertial drift and constant basis (Ojeda *et al.* 2004). In the Mars Pathfinder (MPF) and the rover Sojourner missions, the localization error was found to be ~10% of walking range (Ali *et al.* 2005), and a large localization error is inevitable in the case of wheel slippage and long-term drift (Maimone *et al.* 2006). Celestial navigation (Ning *et al.* 2011) can provide the information of attitude and position regardless of time and distance, whereas it is susceptible to the varied atmosphere of Mars and cannot output the velocity information. In the MER mission, a wheel odometry and an IMU were jointly utilized to estimate rover positions and attitudes with a designed accuracy of 10%, sun sensors were adopted to determine the rover azimuth with an error of $\pm 3^\circ$ (Tebi-Ollennu *et al.* 2001). As a global absolute positioning method, radio measurement neither drifts with time nor be affected by environment (Li *et al.* 2014). Both MER and MSL mission have verified the localization effect of radio measurements, and the localization errors are not larger than ~10 m (Li *et al.* 2004). Visual navigation, as an optical relative navigation, is more suitable for obstacle detection and path planning in short range (Se *et al.* 2004, Li *et al.* 2007, Souvannavong *et al.* 2010). There are some deuterogenic methods developed based on visual navigation, such as Visual Odometry (VO) (Cheng *et al.* 2005) and Bundle Adjustment (BA) (Li *et al.* 2005, Di *et al.* 2002), etc. The former reduced the localization error to ~3% of the range walked, and the latter achieved the localization accuracy of 0.2% of the distance traveled, but their massive computing must rely on the Earth station. Terrain matching localization can obtain the rover's position on a satellite map, and its accuracy heavily depends on the resolution of matching image. The resolution of orbital images obtained by Mars Global Surveyor (MGS), Mars Reconnaissance Orbiter (MRO) and Mars Express (MEX) are partially ~10 m, and the High Resolution Imaging Science Experiment (HiRISE) camera even has acquired unprecedented high-precision image with the resolution of 0.25 m (Carle *et al.* 2010, Li *et al.* 2011, Di *et al.* 2005, Hwangbo *et al.* 2009).

The aim of this paper is to develop a multi-information fusion based autonomous high-precision localization algorithm that can meet the requirements of future Mars rover mission. It is acknowledged that a variety of localization technologies mentioned above do contribute to rover localization, but many of them may not be applied directly to the future Mars rover mission which requires long-time and high-precision navigating independently. The roaming localization of Mars rover only relies on the on-board computer for calculation (Bajracharya *et al.* 2008, Di *et al.* 2008, Wang 2008, Karahayit 2010, Gong 2013). In this paper, the radio measurement between Mars rover and the orbiter(s), the results of terrain image matching, and the output of gyro are introduced as the external measurements to correct the accelerometer constant bias and drift.

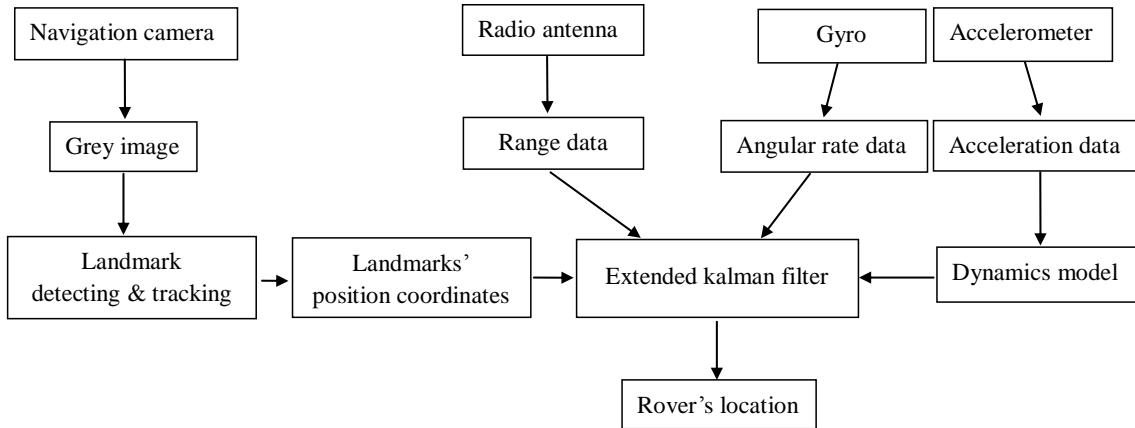


Fig. 1 Multi-information fusion based localization scheme for Mars rover

Multi-information fusion based localization scheme for Mars rover is shown in figure 1. First, the output of the accelerometer is included into the system equation to construct the dynamic model of Mars rover. Then, the output of gyro is considered to get the attitude angles, the radio measurement is introduced to obtain the relative distance between the rover and orbiter, and the line-of-sight of the rover relative to landmarks through the terrain image matching based on camera images and orbital images. Finally, the extended Kalman filter (EKF) is adopted to realize multiple information fusion and high-precision positioning for Mars rover.

2. System modeling

2.1 Coordinate systems

In order to describe the relative geometrical relationship between Mars rover and landing site as well as define the proposed navigation scheme and Mars rover dynamic model, the following three coordinate systems are needed.

2.1.1 Mars center inertial coordinate system (Σ^I)

The origin of the Mars center inertial coordinate system $o_I-x_Iy_Iz_I$ is centered on Mars, and the z_I axis is aligned with the rotation axis of Mars, the x_I axis is defined to point toward the vernal equinox. The y_I axis completes the right-handed orthogonal coordinate system. The orbiter's position and velocity parameters used for the multi-information fusion based localization algorithm are described in the Mars center inertial coordinate system.

2.1.2 Navigation coordinate system (Σ^N)

Given that Mars rover's range of motion is very limited, the issue of Mars rover localization can be described as a relative positional relationship with the landing site, and then the Mars rover's global position can be inferred by the global position of landing site. To this end, the navigation coordinate system $o_N-x_Ny_Nz_N$ is defined as a local inertial frame, whose origin is centered at the landing site. The x_N, y_N, z_N axis of navigation coordinate system is defined to point toward the east,

north, and sky, respectively. The navigation coordinate system is also called East-North-Up (ENU) coordinate system. The Mars rover's position and velocity parameters are described in the navigation coordinate system.

2.1.3 Body-fixed coordinate system (Σ^B)

The origin of body coordinate system $O_B-x_B y_B z_B$ lies in the Mars rover's mass center, three body axis of symmetry are defined as three coordinate axes x_B, y_B, z_B respectively. For simplicity, both of the measurements from inertial measurement unit (IMU) and navigation camera are described in the body-fixed coordinate system.

2.2 Coordinate transformation matrix

According to coordinate systems defined aforementioned, the coordinate transformation matrix \mathbf{T}_B^N from the Mars rover body coordinate system Σ^B to the navigation coordinate system Σ^N is obtained as follows (Ning *et al.* 2011)

$$\mathbf{T}_B^N = \begin{bmatrix} \cos \varphi \cos \psi - \sin \varphi \sin \psi \sin \theta & -\sin \psi \cos \theta & \cos \psi \sin \varphi + \sin \psi \sin \theta \cos \varphi \\ \cos \varphi \sin \psi + \sin \varphi \cos \psi \sin \theta & \cos \psi \cos \theta & \sin \psi \sin \varphi - \cos \psi \sin \theta \cos \varphi \\ -\cos \theta \sin \varphi & \sin \theta & \cos \theta \cos \varphi \end{bmatrix} \quad (1)$$

where θ, φ, ψ are the triaxial attitude angle, that is Euler angle, and the rotation sequence $3(\psi)-2(\theta)-1(\varphi)$ is adopted here.

2.3 Mars rover dynamic equations

For the multiple information fusion based on localization scheme proposed in this paper, we suppose that the high-precision 3-dimensional (3D) map of Mars rover mission area has been obtained by Mars orbiter lengthy precision survey in advance. Hence, the issue of Mars rover localization is simplified to determine its two-dimensional latitude and longitude coordinates. For the sake of simplicity, the Mars is assumed to be a uniform sphere. As the outputs of acceleration is utilized to directly construct the Mars rover's state, both east and north components of acceleration are included into Mars rover state equations. The dynamic equations of Mars rover can be represented in the navigation coordinate system as follows (Ning *et al.* 2011, Xie *et al.* 2012)

$$\begin{cases} \dot{\mathbf{p}} = \mathbf{D}\mathbf{v} \\ \dot{\mathbf{v}} = \Xi \left[\mathbf{T}_B^N (\tilde{\mathbf{a}} - \mathbf{b}_a - \zeta_a) \right]_{3 \rightarrow 2} \end{cases} \quad (2)$$

where $\mathbf{p}=[L, \lambda]^T$ is the Mars rover position vector, L is the latitude and λ is the longitude, $\mathbf{v}=[v_L, v_\lambda]^T$ is the Mars rover velocity vector, v_L, v_λ are the north velocity and east velocity on the Mars surface respectively, $\Xi[\cdot]_{3 \rightarrow 2}$ denotes the operator of extracting the first two elements of a vector with three elements, $\mathbf{D} = \begin{bmatrix} 1/R_M & 0 \\ 0 & 1/(R_M \cos L) \end{bmatrix}$, R_M is radius of Mars. $\tilde{\mathbf{a}}$ is the linear accelerometer output along body axes, \mathbf{b}_a is the acceleration bias, ζ_a is the output noise of white Gaussian acceleration.

3. Navigation measurement model

3.1 Gyro measurement model

A gyro is designed to measure rotation rates around three orthogonal axes, the angular rate measured by a gyro is represented as

$$\tilde{\boldsymbol{\omega}} = \boldsymbol{\omega} + \mathbf{b}_\omega + \boldsymbol{\zeta}_\omega \quad (3)$$

where $\tilde{\boldsymbol{\omega}}$ is the gyro output angular rate around body axes, $\boldsymbol{\omega}$ is true angular rate, \mathbf{b}_ω is the angular rate bias, and $\boldsymbol{\zeta}_\omega$ is the white Gaussian angular rate output noise.

To solve the issue of Mars rover 2-D localization, we only need yaw rate $\tilde{\omega}$ measured by gyro as measurement, so the gyro measurement model is defined as follows

$$y_1 = \tilde{\omega} = \omega + b_\omega + \zeta_\omega \quad (4)$$

where ω is true yaw rate, b_ω is the yaw rate bias, and ζ_ω is the white Gaussian yaw rate measurement noise.

3.2 Radio measurement model

The parameters of orbiting radio beacons measured by the deep-space network (DSN) are uploaded to Mars entry vehicle and rover in advance. Generally, the period of radio measurement is very short compared to the period of orbiting radio beacons. Therefore, the impact of perturbation can be neglected here. Then, the position and velocity of an orbiting radio beacon can be obtained in the Mars center inertial coordinate system according to the simple two-body model

$$\frac{d\mathbf{r}_o}{dt} = \mathbf{v}_o \quad (5)$$

$$\frac{d\mathbf{v}_o}{dt} = -\frac{\mu_M}{|\mathbf{r}_o|^3} \mathbf{r}_o \quad (6)$$

where \mathbf{r}_o is the position vector of the orbiting radio beacon, \mathbf{v}_o is the velocity vector of the orbiting radio beacon, both vectors mentioned above are defined in the Mars center inertial coordinate system, μ_M is Mars gravitational constant.

The range measurement between the Mars rover and an observable orbiting radio beacon can be constructed as follows (Li *et al.* 2014)

$$\tilde{R} = R + \zeta_R \quad (7)$$

where ζ_R is the range measurement noise, R is the true distance between the Mars rover and an observable orbiting radio beacon, it can be obtained

$$R = \sqrt{(\mathbf{r} - \mathbf{r}_o)^T (\mathbf{r} - \mathbf{r}_o)} \quad (8)$$

where $\mathbf{r}(\mathbf{r}=f(\mathbf{p}))$ is the position vector of Mars rover, which is a function of \mathbf{p} .

Then, radio measurement model can be rewritten as follows

$$y_2 = \tilde{R} = R + \zeta_R \quad (9)$$

3.3 Navigation camera measurement model

The terrain image information around Mars rover obtained by navigation camera cannot be directly applied to integrated navigation and localization unless being matched with the remote-sensing image, which is obtained by Mars orbiters and stored in on-board computer in advance. A perspective projection model, usually known as the pinhole camera model, is adopted here to simulate navigation camera measurement process. It is assumed that the two effective feature points extracted from the matched image are not in the same line-of-sight have been extracted from the matched image. The coordinates of two object points are obtained from the terrain image matching algorithm, which can be found from many classical textbooks and is not described here. The pinhole camera model projects object point (x_i^c, y_i^c, z_i^c) to pixel point (u_i, v_i) on the mageplane according to the following relations (Wang 2008, Li *et al.* 2007)

$$\begin{cases} u_i = f \frac{x_i^c}{z_i^c} \\ v_i = f \frac{y_i^c}{z_i^c} \end{cases} \quad (i=1,2) \quad (10)$$

where f is the focal length of the navigation camera. Then, navigation camera measurement model can be constructed as follows

$$\mathbf{y}_3 = \tilde{\mathbf{m}} = \mathbf{m} + \zeta_c \quad (11)$$

where $\mathbf{m}^c = \begin{bmatrix} \mathbf{m}_1^c \\ \mathbf{m}_2^c \end{bmatrix}$, $\mathbf{m}_i^c = \begin{bmatrix} u_i \\ v_i \end{bmatrix} = \frac{f}{z_i^c} \begin{bmatrix} x_i^c \\ y_i^c \end{bmatrix}$, $i=1,2$; ζ_c is the navigation camera measurement noise. Essentially, the coordinates of object points are used to obtain the relative position of Mars rover.

4. Navigation filter design

In order to comprehensively utilize the output information of gyro, radio measurement, and results of terrain image matching to estimate Mars rover state variables and suppress navigation measurement noise, and then to realize multiple information fusion based high-precision localization for Mars rovers, the navigation filter is designed by use of the extended Kalman filter.

4.1 System equations

We select $\mathbf{X} = [\mathbf{p}^T, \mathbf{v}^T]^T$ as state variables, where the Mars rover's relative position vector \mathbf{p} and relative velocity vector \mathbf{v} are all defined in the navigation coordinate system.

Then, the Mars rover dynamic equations (Eq. (2)) can be rewritten as follows

$$\dot{\mathbf{X}}(t) = \begin{bmatrix} \mathbf{D}\mathbf{v} \\ \Xi \left[\mathbf{T}_B^N (\tilde{\mathbf{a}} - \mathbf{b}_a - \zeta_a) \right]_{3 \rightarrow 2} \end{bmatrix} = \mathbf{f}(\mathbf{X}(t), t) + \mathbf{w} \quad (12)$$

Similarly, navigation observation equations defined in Eqs. (4), (9) and (11) can also be written as follows

$$\mathbf{Y}(t) = \begin{bmatrix} y_1 \\ y_2 \\ \mathbf{y}_3 \end{bmatrix} = \begin{bmatrix} \tilde{\omega} \\ \tilde{R} \\ \tilde{\mathbf{m}} \end{bmatrix} = \mathbf{h}(\mathbf{X}(t), t) + \mathbf{v} \quad (13)$$

The system equations utilized in the subsequent navigation filter can accordingly be defined as follows

$$\dot{\mathbf{X}}_k = \mathbf{f}(\mathbf{X}_{k-1}) + \mathbf{w}_{k-1} \quad (14)$$

$$\mathbf{Y}_k = \mathbf{h}(\mathbf{X}_k) + \mathbf{v}_k \quad (15)$$

where \mathbf{w}_k and \mathbf{v}_k represent the system process noise and measurement noise respectively, they are assumed to be independent of each other, white and with normal probability distributions

$$p(\mathbf{w}) \sim N(0, \mathbf{Q}) \quad (16)$$

$$p(\mathbf{v}) \sim N(0, \mathbf{R}) \quad (17)$$

$$\text{Cov}(\mathbf{w}_k, \mathbf{v}_j) = \mathbf{E}(\mathbf{w}_k \mathbf{v}_j^T) = 0 \quad (18)$$

Define state transfer matrix $\Phi_{k+1/k}$

$$\Phi_{k/k-1} = \mathbf{I} + \mathbf{F}_{k/k-1} \cdot \Delta t \quad (19)$$

$$\dot{\Phi}(t, \tau) = \mathbf{F}(t) \Phi(t, \tau) \quad (20)$$

$$\Phi(t, t) = \mathbf{I} \quad (21)$$

where \mathbf{F} is the Jacobian matrix of partial derivatives of \mathbf{f} with respect to state variable \mathbf{X} , that is

$$\mathbf{F}_{k/k-1} = \left. \frac{\partial \mathbf{f}(\mathbf{X}, k)}{\partial \mathbf{X}} \right|_{\mathbf{X}=\mathbf{X}_{k-1}} \quad (22)$$

Define sensitivity matrix \mathbf{H}_k

$$\mathbf{H}_k = \left. \frac{\partial \mathbf{h}(\mathbf{X})}{\partial \mathbf{X}} \right|_{\mathbf{X}=\hat{\mathbf{x}}_{k/k-1}} \quad (23)$$

4.2 Extended kalman filter

Initialization: for $k=0$, set

$$\hat{\mathbf{X}}_0 = E[\mathbf{X}_0] \quad (24)$$

$$\mathbf{P}_0 = E\left[(\mathbf{X}_0 - E[\mathbf{X}_0])(\mathbf{X}_0 - E[\mathbf{X}_0])^T\right] \quad (25)$$

EKF time update equations

$$\dot{\hat{\mathbf{X}}}_{k/k-1} = \mathbf{f}(k, \hat{\mathbf{X}}_{k-1}) \quad (26)$$

$$\mathbf{P}_{k/k-1} = \Phi_{k/k-1} \mathbf{P}_{k-1} \Phi_{k/k-1}^T + \mathbf{Q}_{k-1} \quad (27)$$

EKF measurement update equations

$$\mathbf{K}_k = \mathbf{P}_{k/k-1} \mathbf{H}_k^T \left[\mathbf{H}_k \mathbf{P}_{k/k-1} \mathbf{H}_k^T + \mathbf{R}_k \right]^{-1} \quad (28)$$

$$\hat{\mathbf{X}}_{k/k} = \hat{\mathbf{X}}_{k/k-1} + \mathbf{K}_k \left[\mathbf{y}(t_k) - \mathbf{h}(\hat{\mathbf{X}}_{k/k-1}) \right] \quad (29)$$

$$\mathbf{P}_k = (\mathbf{I} - \mathbf{K}_k \mathbf{H}_k) \mathbf{P}_{k/k-1} (\mathbf{I} - \mathbf{K}_k \mathbf{H}_k)^T + \mathbf{K}_k \mathbf{R}_k \mathbf{K}_k^T \quad (30)$$

5. Numerical simulation and analysis

As the focus of this study is not including the motion trajectory planning of Mars rovers, we suppose the rover walk along a randomly generated two-dimensional trajectory on the surface of Mars, which is defined in the navigation coordinate system. The planned simulation time span is assumed to be 1000 seconds, and the sample step is set to 1 second. A four-order Runge-Kutta algorithm is selected as the numerical solver of the integral Mars rover dynamic equations. Other relative parameters used in the simulation are set as follows: Mars gravitational constant $\mu_M=4.282829 \times 10^{13} \text{ km}^3/\text{s}^2$, Mars rotating angular rate $\omega_M=7.0882 \times 10^{-5} \text{ rad/s}$; According to the parameters of IMU used in the Mars Exploration Rover (MER) mission, the accelerometer bias \mathbf{b}_a and gyro bias \mathbf{b}_ω adopted in the simulation are assumed to be $[3 \times 10^{-3}, 3 \times 10^{-3}, 3 \times 10^{-3}] \text{ m/s}^2$ and $[5 \times 10^{-6}, 5 \times 10^{-6}, 5 \times 10^{-6}] \text{ rad/s}$ respectively, the covariance matrix of white Gaussian noise ζ_a and ζ_ω are set to $[5 \times 10^{-8}, 5 \times 10^{-8}, 5 \times 10^{-8}] \text{ (m/s}^2\text{)}^2$ and $[9 \times 10^{-8}, 9 \times 10^{-8}, 9 \times 10^{-8}] \text{ (rad/s)}^2$ respectively.

Initial state \mathbf{X}_0 is assumed as

$$\mathbf{X}_0 = [0, 0, 0.1, 0.1]^T$$

Initial state error covariance matrix \mathbf{P}_0 is assumed as:

$$\mathbf{P}_0 = \begin{bmatrix} 10^2 \mathbf{I}_{2 \times 2} & \\ & \mathbf{I}_{2 \times 2} \end{bmatrix}_{4 \times 4}$$

System process noise variance matrix \mathbf{Q} is assumed as:

$$\mathbf{Q} = \begin{bmatrix} 25 \cdot \mathbf{I}_{2 \times 2} & \\ & 4 \cdot \mathbf{I}_{2 \times 2} \end{bmatrix}_{4 \times 4}$$

Measurement noise covariance matrix \mathbf{R}_k is assumed as:

$$\mathbf{R}_k = \begin{bmatrix} 9 \times 10^{-8} & & \\ & 10 & \\ & & 10^{-6} \mathbf{I}_{2 \times 2} \end{bmatrix}_{4 \times 4}$$

To comprehensively validate the effectiveness of the localization scheme proposed in this paper and explore the impact of satellite image resolution and accuracy of radio measurement on localization results, four simulation cases are implemented with different parameter setting. According to the scientific data from MGS, MRO, HiRISE, MER and MSL missions, the four cases of simulation parameters are given out in Table 1, and the corresponding simulation results are shown in Figs. 2-9. Since there is no drift in both the image and radio measurements, the multi-information fusion based localization scheme for Mars rovers can effectively correct the inertial constant bias and drift, thus the accuracy of localization is improved.

Computer simulation is firstly performed under the condition of case 1. As shown in Fig. 2 and

Table 1 Four cases of simulation parameters

Simulation case \ Parameters	Resolution of satellite image (m)	Accuracy of radio measurement (m)
Simulation case 1	10	10
Simulation case 2	10	1
Simulation case 3	0.25	10
Simulation case 4	0.25	1

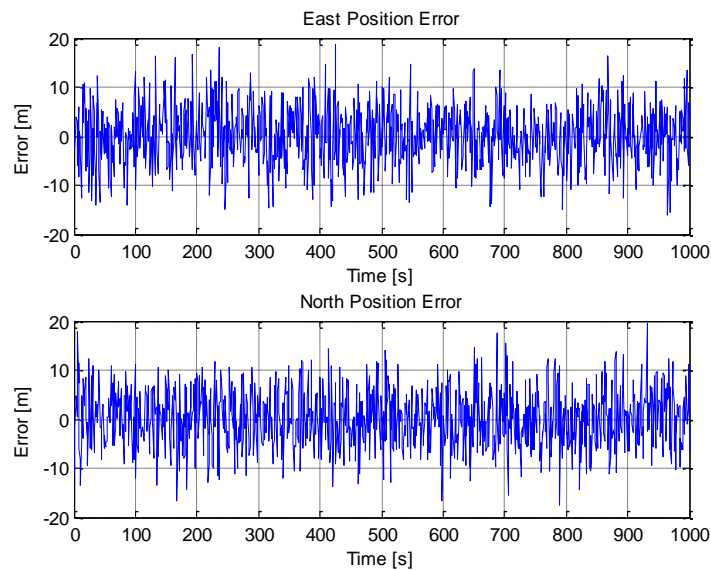


Fig. 2 East and north position errors of simulation case 1

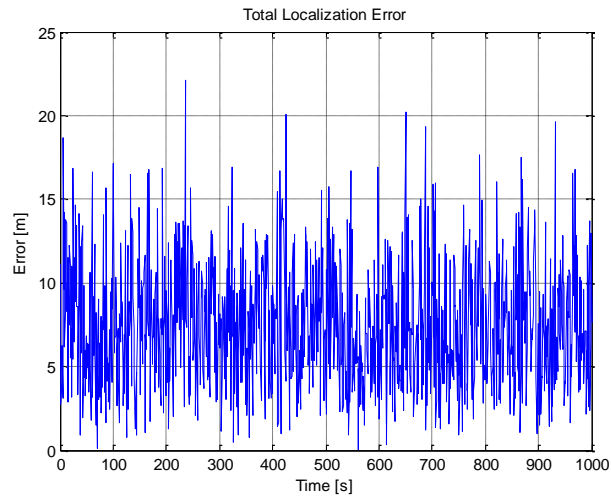


Fig. 3 Total localization errors of simulation case 1

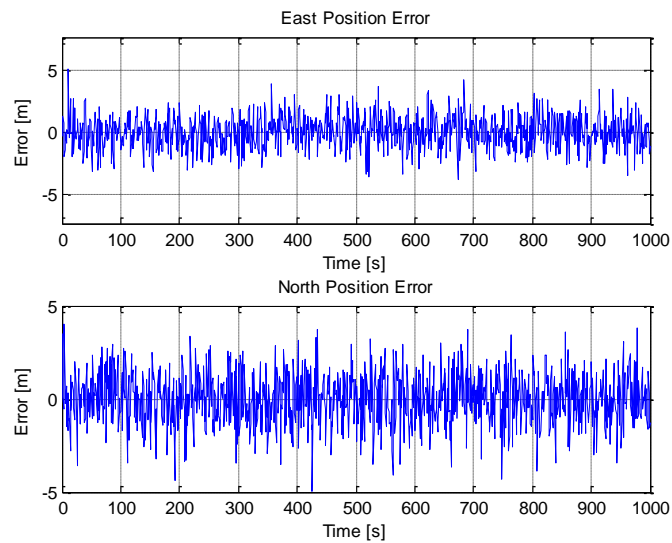


Fig. 4 East and north position errors of simulation case 2

Fig. 3, the accuracy of the localization scheme developed in this paper is about 20 m and approximately equivalent to that of inertial navigation under the conditions of lower resolution of satellite image and lower accuracy of radio measurement. Because there are not drift and errors accumulation in both the terrain image matching and radio measurement, these two external measurements are primarily utilized to suppress the divergent of inertial navigation errors. Therefore, it is unnecessary to add external sensors to IMU in this case, which is an important reason for integrated navigation and localization scheme was not used in early Mars rover missions. Obviously, it is not able to meet the localization accuracy requirement of future Mars rover missions.

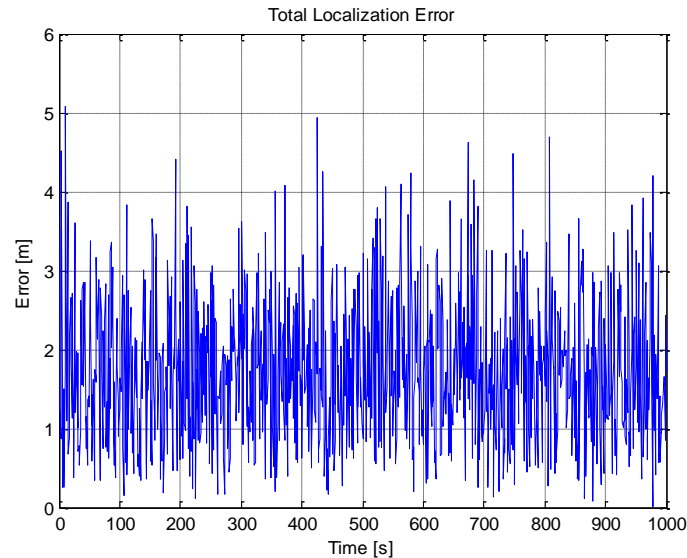


Fig. 5 Total localization errors of simulation case 2

Secondly, we improved the accuracy of radio measurement up to 1 m and adopted the same lower resolution satellite image used in case 1. The east and north position errors, and total error are shown in Fig. 4 and Fig. 5 respectively. In this case, the radio measurement becomes the primary external measurement to correct the inertial constant basis and drift, while the lower resolution of satellite image leads to large measurement noise. It can be seen from Fig. 4 and Fig. 5 that the application of the extended Kalman filter not only suppresses the inertial drift and error accumulation, but also improves the localization accuracy significantly. The localization error is reduced within 5 m in the simulation case 2, which can basically meet the localization accuracy requirement for roaming exploration of recent Mars rover missions.

Next, we tried to improve the resolution of satellite image up to 0.25 m and adopt the radio measurement used in case 1 with the same lower accuracy. The east and north position errors, and total error are given out in Fig. 6 and Fig 7 respectively. It is easily concluded from the Fig 6 and 7 that the localization error is reduced compared to simulation case 1 and kept within 2 m, which can basically meet the localization accuracy requirement for future roaming exploration. In this simulation case, the terrain image matching navigation measurement is considered as the primary external measurement and fed into extended Kalman filter in order to correct the basis and drift and improve the accuracy of navigation and localization. It should be noticed from Figs 5 and 7 that the localization accuracy of simulation case 3 is improved from 5m to 2m when compared to that of simulation case 2. Therefore, we can safely conclude that the resolution of satellite image has the greater impact to the total localization accuracy when compared with the accuracy of radio measurement.

Finally, we tested the performance of the localization algorithm proposed in this paper under the simulation case 4. As before, the east and north position errors, and total error are depicted in Fig. 8 and Fig. 9 respectively. Because the satellite image and radio measurement with high accuracy are utilized and considered as external measurements included into the navigation filter, the inertial drift and error accumulation can be effectively suppressed and corrected, therefore, the

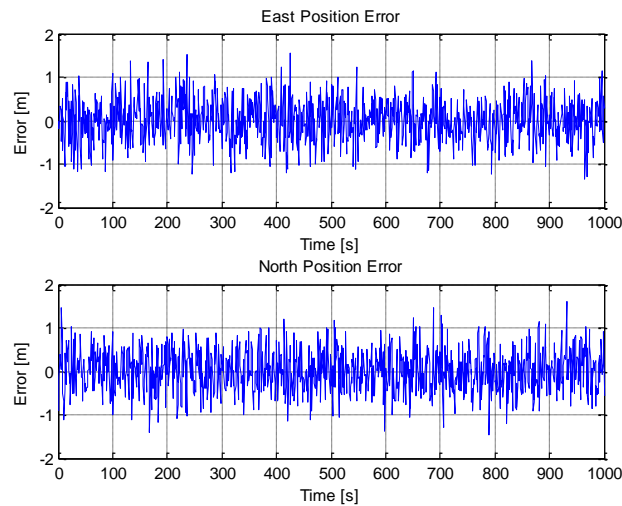


Fig. 6 East and north position errors of simulation case 3

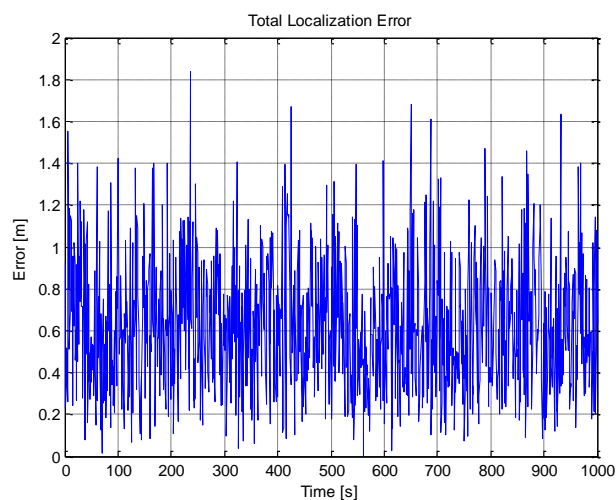


Fig. 7 Total localization errors of simulation case 3

Mars rover localization accuracy has been greatly improved. It can be found from Figs. 8 and 9 that the localization error is reduced within 35 cm under the simulation case 4, which can completely meet the localization accuracy requirement for both roaming exploration and settling investigation.

It should be noticed from Fig. 9 that the localization error is inferior to the resolution of satellite image in the simulation case 4. The same phenomenon can also be found in the simulation case 3. The reason why the multi-information fusion based localization errors are inferior to the resolution of satellite image maybe lies in the following aspects. Firstly, the performance of EKF usually degrades due to the serious nonlinearity in the dynamic equations and navigation measurement model. Secondly, the drift and noise from system model and external measurements are a bit

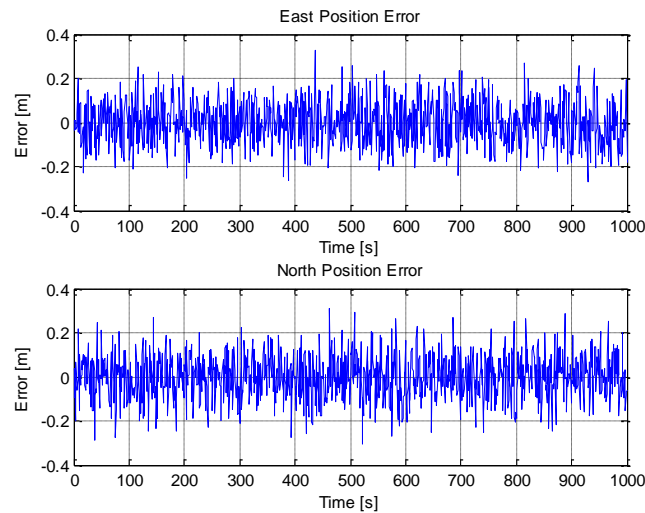


Fig. 8 East and north position errors of simulation case 4

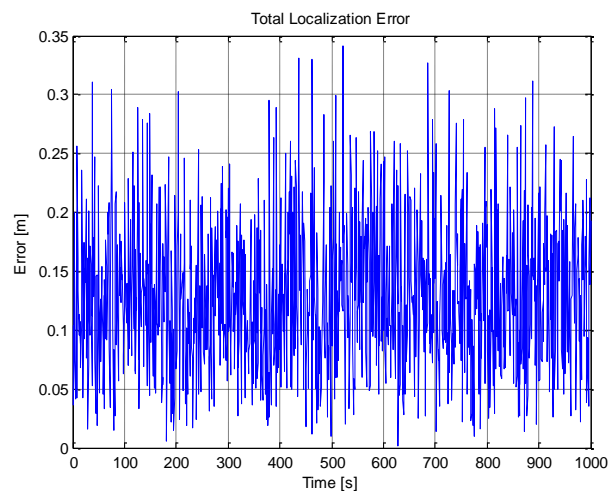


Fig. 9 Total localization errors of simulation case 4

difficult to be effectively suppressed by the navigation filter. Last not least, both the external measurements and position of Mars rover are defined in the different coordinate systems, which must be transferred into the same coordinate system in order to perform the navigation filter. Many factors, such as the rotation of Mars, non-ideal sphere, complex terrain, will affect the computational accuracy of the coordinate transform and result in a considerable deviation. For these reasons, the localization accuracy is close to but a bit lower than the resolution of satellite image in the simulation case 3 and 4.

Di *et al.* discussed the Mars rover positioning problem utilizing the high-resolution satellite images. A lot of match points are required in order to achieve a higher localization accuracy (Di *et al.* 2011). Due to the limited computing capability onboard, the localization algorithm based on

multiple feature points matching and tracking is difficult to apply in the engineering practice. To accommodate the limited capabilities of on-board computer, only two feature points are utilized in the localization algorithm developed in this paper.

6. Conclusions

The capability of autonomous roaming exploration is the cornerstone for future Mars rover missions. High-precision localization is considered as one of the required key technologies to achieve autonomous roaming exploration. This paper addresses an innovative high-precision Mars rover localization algorithm based on radio measurements, terrain image matching, and inertial measurement using a multi-information fusion approach. The radio measurement and the terrain image matching are introduced as the navigation observables to correct the inertial constant bias and drift and then improve the localization accuracy of Mars rovers. Simulation results show that the resolution of satellite image and accuracy of radio measurement will directly affect the localization accuracy of the scheme. In the case of the high-precision terrain image matching and the radio measurement, the total localization error is less than 35 cm, which can meet localization accuracy requirement of the future Mars roaming exploration.

The localization algorithm developed in this paper is a two-dimensional localization scheme. In order to obtain the rover's three-dimensional position, the high-resolution three-dimensional terrain image of the Mars rover mission area must be pre-stored into the on-board computer. At the same time, the localization algorithm developed in this paper requires at least one orbiter to provide radio measurement during the Mars rover mission. In engineering practice, the unforeseen circumstances, such as the blackout of radio measurement or failure of image matching, may appear during the localization operation process of Mars rovers, which inevitably disable the navigation and localization of Mars rovers. Both the issues mentioned above should be carefully addressed in the further study.

Acknowledgments

The work described in this paper was supported by the National Natural Science Foundation of China (Grant No. 61273051), Innovation Funded Project of Shanghai Aerospace Science and Technology (Grant No. SAST201213), the Fundamental Research Funds for the Central Universities (Grant No. NS2014094), and the Foundation of Graduate Innovation Center in NUAU (Grant No. kfjj130135). The author fully appreciates their financial supports.

References

- Bajracharya, M., Maimone, M.W. and Helmick, D. (2008), "Autonomy for mars rovers: past, present, and future", *Computer*, **41**(12), 44-50.
- Di, K., Wang, J., He, S., Wu, B., Chen, W., Li, R. and Howard, A.B. (2008), "Towards autonomous mars rover localization: Operations in 2003 MER mission and new developments for future missions", *Int. Arch. Photogramm. Remote Sens.*, **37**, 957-962.
- Wang, J. (2008), "Modeling and matching of landmarks for automation of Mars rover localization", Ph.D. Dissertation, The Ohio State University.

- Karahayit, O. (2010), "Mars exploration rover mission-rover localization and topographic mapping", Master Dissertation, The Ohio State University.
- Gong, W. (2013), "Potential of MSL rover localization compared with MER", Ph.D. Dissertation, The Ohio State University.
- Ojeda, L., Reina, G. and Borenstein, J. (2004), "Experimental results from FLEXnav: An expert rule-based dead-reckoning system for Mars rovers", *Proceedings of the 2004 IEEE Aerospace Conference*, March.
- Ali, K.S., Vanelli, C.A., Biesiadecki, J.J., Maimone, M.W., Cheng, Y., San Martin, A.M. and Alexander, J.W. (2005), "Attitude and position estimation on the Mars exploration rovers", *Proceedings of the 2005 IEEE International Conference on Systems, Man and Cybernetics*, October.
- Maimone, M., Johnson, A., Cheng, Y., Willson, R. and Matthies, L. (2006), *Autonomous Navigation Results From the Mars Exploration Rover (MER) Mission*, Springer Berlin Heidelberg.
- Ning, X.L., Cai, H.W., Wu, W.R., Fang, J.C. and Zhang, X.L. (2011), "INS/CNS integrated navigation method for lunar rover", *Syst. Eng. Electr.*, **33**(8), 1837-1844.
- Trebi-Ollennu, A., Huntsberger, T., Cheng, Y., Baumgartner, E.T., Kennedy, B. and Schenker, P. (2001), "Design and analysis of a sun sensor for planetary rover absolute heading detection", *IEEE Tran. Robot. Autom.*, **17**(6), 939-947.
- Li, S., Jiang, X. and Liu, Y. (2014), "High-precision Mars entry integrated navigation under large uncertainties", *J. Navigation*, **67**, 327-342.
- Li, R., Di, K., Matthies, L.H., Arvidson, R.E., Folkner, W.M. and Archinal, B.A. (2004), "Rover localization and landing-site mapping technology for the 2003 Mars Exploration Rover mission", *Photogram. Eng. Remote Sens.*, **70**(1), 77-90.
- Se, S., Ng, H.K., Jasiobedzki, P. and Moyung, T.J. (2004), "Vision based modeling and localization for planetary exploration rovers", *Proceedings of 55th International Astronautical Congress*, October.
- Li, S., Cui, P. and Cui, H. (2007), "Vision-aided inertial navigation for pinpoint planetary landing", *Aeros. Sci. Tech.*, **11**(6), 499-506.
- Souvannavong, F., Lemaréchal, C., Rastel, L., Maurette, M. and Magellium, F. (2010), "Vision-based motion estimation for the ExoMars rover", *International Symposium on Artificial Intelligence, Robotics and Automation in Space (iSAIRAS)*, Sapporo, Japan.
- Cheng, Y., Maimone, M. and Matthies, L. (2005), "Visual odometry on the Mars exploration rovers", *Proceedings of the 2005 IEEE International Conference on Systems, Man and Cybernetics*, October.
- Li, R., Di, K., Wang, J., Agarwal, S., Matthies, L., Howard, A. and Willson, R. (2005), "Incremental bundle adjustment techniques using networked overhead and ground imagery for long-range autonomous mars rover localization", *Proceedings of ISAIRAS 2005 Conference*, August.
- Di, K., Xu, F., Li, R., Matthies, L.H. and Olson, C.F. (2002), "High precision landing site mapping and rover localization by integrated bundle adjustment of MPF surface images", *Int. Arch. Photogram. Remote Sens. Spatial Inform. Sci.*, **34**(4), 733-737.
- Carle, P.J., Furgale, P.T., and Barfoot, T.D. (2010), "Long-range rover localization by matching LIDAR scans to orbital elevation maps", *J. Field Robot.*, **27**(3), 344-370.
- Li, R., He, S., Chen, Y., Tang, M., Tang, P., Di, K. and Sims, M. (2011), "MER spirit rover localization: comparison of ground image-and orbital image-based methods and science applications", *J. Geophys. Res.*, **116**, E00F16, doi:10.1029/2010JE003773.
- Di, K., Xu, F., Wang, J., Niu, X., Serafy, C., Zhou, F. and Matthies, L. (2005), "Surface imagery based mapping and rover localization for the 2003 Mars Exploration Rover mission", *Proceeding of ASPRS 2005 Annual Conference*, Baltimore, Maryland, March.
- Xie, L., Yang, P., Yang, T. and Li, M. (2012), "Dual-EKF-based real-time celestial navigation for lunar rover", *Mathematical Problems in Engineering*, 2012, Article ID 578719, doi:10.1155/2012/578719.
- Di, K., Liu, Z. and Yue, Z. (2011), "Mars rover localization based on feature matching between ground and orbital imagery", *Photogram. Eng. Remote Sens.*, **77**(8), 781-791.